Dynamical Climatology

Simulation of the seasonal cycle of SST using globally specified climatological data to force simple ocean models.

by

N.S. Grahame

DCTN 5

September 1984

Meteorological Office (Met. O. 20)
London Road
Bracknell
Berkshire RG12 2SZ

DYNAMICAL CLIMATOLOGY TECHNICAL NOTE NO. 5

SIMULATION OF THE SEASONAL CYCLE OF SST USING GLOBALLY SPECIFIED CLIMATOLOGICAL DATA TO FORCE SIMPLE OCEAN MODELS

by

N S GRAHAME

Met O 20 (Dynamical
Climatology Branch)
Meteorological Office
London Road
Bracknell
Berkshire RG12 2SZ

September 1984

1. Introduction

This note describes a series of global experiments performed using climatologically specified fluxes to force simple single column models of the upper ocean. A slab model is used initially with subsequent modifications to include a representation of advective heat flux and a seasonal variation of the mixed layer depth. Despite the nature of the approximations it is found that a modified slab model can reproduce the broad scale features of the seasonal cycle over much of the ocean outside the Tropics with tolerable realism using this forcing.

These experiments are designed to provide a set of preliminary results with which future simulations using more complex ocean models can be compared. They also give a useful insight into some of the factors which govern seasonal changes in sea surface temperature (SST).

2. Rationale for using observed data

Numerical modelling of the coupled ocean-atmosphere system is in a development stage at present. As part of the process of developing a fully coupled ocean-atmosphere general circulation model in Met O 20, a number of short experiments have been carried out in both an interactive and non-interactive context using atmospheric general circulation model (AGCM) fluxes to force a Kraus-Turner type mixed layer model. In these experiments the seasonal cycle of SST has been on the whole well represented in the Southern hemisphere but there have been large deviations from climatology in the Northern hemisphere. These problems have been extensively discussed in Gordon and Bottomley (1984). Use of AGCM forcing would normally be expected to give a less realistic simulation of SST than would use of observed data and it is pertinent to carry out simulations forced by observed data for eventual comparison with those using model forcing.

There have been a few attempts to simulate the global seasonal cycle using observed climatological data. These have been limited, however, by the lack of relevant forcing fluxes in a form suitable for use in such studies. Kim and Gates (1980) used an imbedded mixed layer in a dynamical ocean model and specified climatological forcing using data from Schutz and Gates (1971 to 1974) to provide the heat fluxes and Hellerman (1967) for seasonal values of the windstress components from which estimates of mixing energy were made. It seems likely that mixing energy based on time-meaned

windstress values will be underestimated since the variability of the wind forcing is not being adequately represented (Grahame, 1984). Simulated mixed layer temperatures obtained from this experiment exhibited large deviations from climatology in some areas but Kim and Gates claimed that the seasonal cycle of SST was reasonably represented.

More recently, Esbensen and Kushnir (1981) have produced datasets containing monthly mean surface heat budget components and other variables relating to the global ocean. These have an obvious use in providing a climatological forcing for ocean model simulations and for verifying surface fluxes from atmospheric model data. There will be shortcomings, of course, in these data; the authors point out that values in data sparse areas should be viewed with some caution. Nevertheless the datasets do provide the most reliable source of information over the global ocean at the present time. In this note we use these datasets as reference forcing and apply them to simple ocean models in an attempt to underline some of the important factors which govern the seasonal evolution of SST over the global ocean and to gain some further feel for their quality.

In what follows we shall find it useful to take the climatological range of SST as a measure of the amplitude of the seasonal cycle.

3. Climatological seasonal range of SST

The climatological range of SST is shown in Figure 1 where it is defined as

$(\overline{T}_{AUG} - \overline{T}_{MAR})$ in the Northern hemisphere

$(\overline{T}_{FEB} - \overline{T}_{SEP})$ in the Southern hemisphere

$\overline{T}$ denotes a monthly mean SST and values have been taken from Esbensen and Kushnir (1981). The use of monthly means will inevitably underestimate the "true" climatological range but the definition is used to enable direct comparisons to be made with the simulated results presented later. (N.B. The seasonal range as defined here gives a discontinuity at the Equator when plotted on a global map). The seasonal range maxima occur at middle latitudes in both hemispheres where there is a strong seasonal signal in the surface forcing fluxes. Apart from the boundary current regions of the Gulf Stream and Kuroshio, the largest ranges are found in the mid-North Pacific (greater than 9°C using the above definition). It is interesting to note that the corresponding maxima in the Southern hemisphere are only of order 6°C. We shall see later that the seasonal range amplitude and

summer-time mixed layer depth tend to be inter-related in mid-latitude regions. In the Tropics, the definition of seasonal range becomes somewhat arbitrary and is complicated by the fact that relatively large interannual variations of SST can take place. There is little seasonal variation in the Western Pacific but changes do occur in the Equatorial Eastern Pacific with the development of a cold water tongue which reaches its maximum intensity during September and October.

4. One dimensional modelling of the upper ocean mixed layer

Figure 2 shows an observed temperature profile of the upper ocean for a summer situation in the mid-latitude North Pacific. The diagram shows three distinct regions

(i) a mixed (isothermal) layer extending from the surface to ~25m

(ii) the seasonal thermocline

(iii) the permanent thermocline.

Over the seasonal cycle the mixed layer depth varies from less than 25m in summer to perhaps greater than 200m in winter at mid-latitudes. The seasonal thermocline is a region of large temperature gradient bounded by the mixed layer base and a depth where seasonal changes in temperature no longer occur. Below this depth the temperature continues to decrease with depth to about 1.5 km. This region is known as the permanent thermocline. At greater depths there is little temperature gradient in the vertical.

Bulk models of the ocean mixed layer are essentially based on equations for the rate of change of heat and turbulent kinetic energy integrated over the water column. The potential energy of the water column will change if changes in heat content occur and if heat is redistributed by mechanical mixing processes. The mixing involves the conversion of turbulent kinetic energy to potential energy and can be generated either internally or externally by a number of different processes (e.g. internal waves, local wind-induced mixing). For the purposes of this note it suffices to say that, on the temporal and spatial scales considered here, the dominant mechanism for mixing is the action of the wind on the ocean surface which can be appropriately scaled in terms of the cube of the atmospheric friction velocity, u_*^3 (Kraus and Turner, 1967, DeSzoeke and Rhines, 1976).

A version of the Kraus-Turner bulk mixed layer model developed by Mitchell (1977a) has been used in the Met O 20 Ocean Modelling Group to investigate aspects of the seasonal cycle of SST. During the summer months the SST becomes particularly sensitive to the mixed layer depth, h, as the layer itself shallows. Under these conditions the depth is essentially determined by a balance between net heat input (acting to stabilise and shallow the layer) and the turbulent kinetic energy input from the wind, which mixes the surface heat downwards thereby converting the turbulent kinetic energy to potential energy. During the winter, convective overturning caused by surface heat loss leads to a deepening of the mixed layer. To specify the turbulent mixing by wind forcing over monthly periods one ideally needs global datasets of accumulated monthly mean mixing energy. The quantity can be expressed with reasonable accuracy in terms of the monthly mean windspeed and variance. At the time these experiments were performed only global datasets of the former were available and it has been shown that estimates based on the monthly mean windspeed alone do not adequately represent the wind forcing (Grahame, 1984). The experiments described here are therefore based entirely on what can be deduced from the mixed layer heat conservation equation. However potential energy changes can be included implicitly as will be seen later. During deepening the entrainment of colder water from below the layer is important in the mixed layer heat budget. In the simple models to be described we have no information regarding the temperature profile below the layer. We shall therefore only consider the case when the mixed layer is shallowing although in the next section the entrainment term is included for the sake of completeness.

4.1 Model formulation

The heat equation can be written as

$$\frac{\partial T}{\partial t} + \underline{U}.\underline{\nabla} T + W\frac{\partial T}{\partial z} = \frac{\partial}{\partial z}\left(-\overline{W'T'}\right) + \frac{1}{c\rho_o}\frac{\partial I(z)}{\partial z} \qquad (1)$$

where $\overline{W'T'}$ is the time-meaned turbulent heat flux (which is assumed to be zero in the quiescent fluid below the mixed layer) and I(z) is the penetrative part of the solar flux. We now consider this equation in the context of numerical modelling of the upper ocean. Figure 3 shows the temperature and velocity profiles on which the following equations are

based. Firstly if equation (1) is integrated from the surface to just above the mixed layer base ($z = -h + \Delta h/2$) then in the limit $\Delta h \to 0$ one can obtain an equation for changes in mixed layer temperature

$$h\frac{\partial T_m}{\partial t} + h\,(\underline{U}_g + \underline{U}_e).\underline{\nabla}T_m = \frac{Q}{c\rho_o} - [-\overline{W'T'}]|_{-h+\Delta h/2} \qquad (2)$$

where $Q = c\rho_o\,[-\overline{W'T'}]|_o + I_o$ is the net heat flux at the surface. (The penetrative component is assumed to be completely absorbed within the mixed layer). If we now integrate equation (1) across the transition zone then the turbulent heat flux at the base of the mixed layer is given by (Gordon, 1984)

$$[-\overline{W'T'}]|_{-h+\Delta h/2} = \epsilon\, W_E\, \Delta T$$

where W_E is the entrainment velocity $\equiv \left(\frac{dh}{dt} + W_{-h}\right)$

$\Delta T = T_{-h+\Delta h/2} - T_{-h-\Delta h/2}$

and $\epsilon = 1;\ W_E > 0$; $\frac{d}{dt} = \frac{\partial}{\partial t} + (\underline{U}_g + \underline{U}_e).\nabla$
$\quad\ 0;\ W_E \leq 0$

Equation (2) can therefore be written as

$$h\frac{\partial T_m}{\partial t} + h\,(\underline{U}_g + \underline{U}_e).\underline{\nabla}T_m = \frac{Q}{c\rho_o} - \epsilon W_E \Delta T \qquad (3)$$

Finally for changes in <u>heat content</u> from just below the mixed layer ($z = -h - \Delta h/2$) to $-d$, then for $\Delta h \to o$, equation (1) becomes

$$\left[\frac{\partial}{\partial t} + \underline{U}_g.\underline{\nabla}\right]\int_{-d}^{-h-\Delta h/2} T\,dz + \left[\frac{\partial h}{\partial t} + \underline{U}_g.\underline{\nabla}h\right]T_{-h-\Delta h/2} + W_{-h}\,(T_{-h-\Delta h/2} - T_{-d}) = 0 \qquad (4)$$

assuming the depth, $-d$, is constant.

To obtain an equation for changes in heat content above the permanent thermocline we re-write (3) in terms of heat content of the mixed layer and add to (4), again taking the limit $\Delta h \to 0$

$$\frac{\partial H}{\partial t} = h\,\underline{U}_e.\underline{\nabla}T_m + \underline{U}_g.\underline{\nabla}\int_{-d}^{0} T dz + W_{-h}(T_m - T_{-d}) - \Delta T(\underline{U}_e.\underline{\nabla}h) = \frac{Q}{c\rho_o} \qquad (5)$$

where H is the heat content above the permanent thermocline $\left[\int_{-d}^{o} T dz\right]$.

Numerical experiments performed by Wells (1979) suggest that the last term on the left-hand side of (5), involving the horizontal advection of h by Ekman currents, can be ignored. If each term is split into an annual mean and seasonally varying part ($X = \overline{X} + X'$) then for the former

$$\frac{\partial \overline{H}}{\partial t} + \overline{h(\underline{U}_e.\underline{\nabla}T_m)} + \overline{\underline{U}_g.\underline{\nabla}\int_{-d}^{o} T dz} + \overline{W_{-h}\,(T_m - T_{-d})} = \frac{\overline{Q}}{c\rho_o} \qquad (6)$$

For seasonal variations

$$\frac{\partial H'}{\partial t} = \frac{Q'}{c\rho_o} - (h\,\underline{U}_e.\underline{\nabla}T_m)' - (\underline{U}_g.\underline{\nabla}\int_{-d}^{o} T dz)' - [\,W_{-h}\,(T_m - T_{-d})]' = 0 \qquad (7)$$

Gill and Niiler (1973) show that, in mid-latitude open ocean regions, large scale seasonal changes of heat content in the upper ocean are primarily determined by the seasonal component of the net surface heat flux. However, horizontal Ekman transports can be important in the mixed layer heat budget if the layer is shallow. Equations (3), (5) and (6) are central to the discussion which follows.

4.2 Data used for climatological forcing

The following data fields were extracted from Esbensen and Kushnir (1981):

Available solar heat flux - using Berliand's formula as presented by Budyko (1974) with albedo also considered (F_S)

Net long-wave radiation - as derived by the above authors from Berliand's formulation (F_I)

Latent heat flux and sensible heat flux - evaluated using bulk formulae (F_{LH} and F_{SH}).

The above quantities are given by Esbensen and Kushnir as monthly means on a 4° x 5° regular latitude/longitude grid and, added together, provide an estimate of the net surface heat flux

$$Q = F_S + F_I + F_{SH} + F_{LH} \qquad (8)$$

The data were interpolated onto a 2.5° x 3.75° grid to enable the results from these experiments to be compared directly to other experiments performed in Met O 20.

5. Description of the experiments and results

In this section a set of sensitivity experiments is described whereby the climatologically specified fluxes are used to force some simple models of the upper ocean. We are generally interested in how well the broad features of the seasonal cycle of SST can be represented over the global ocean but will concentrate on mid-latitude open ocean regions where local forcing is important in determining seasonal heat content changes. Since we are considering the case when the mixed layer is shallowing, the entrainment flux term in equation (3) can be ignored (ϵ=0). The models have been run over the respective heating season of each hemisphere starting from March climatological SSTs in the Northern hemisphere and September climatological SSTs in the Southern hemisphere (assumed to be representative mid-monthly values in each case). The simulated seasonal range of SST from each experiment is compared to the climatological seasonal range and the differences discussed. The definition of seasonal range used here has already been referred to in Section 3. When analysing results from these experiments one must be aware that a cancellation of errors could provide a reasonable simulation. It is therefore important to understand how well the processes involved are being represented.

A. Uniform depth ocean - slab model

This is the simplest model which can be used to represent heat storage in the ocean and has the following constraints

a) the mixed layer depth, h, is taken to be constant spatially and temporally (h_s)

b) all advective effects are ignored.

The value of h_s is taken to be 68m which represents a global mean effective depth of the seasonal thermocline (see Manabe and Stouffer, 1980). At each ocean grid-point, equation (3) becomes simply

$$\frac{\partial T_m}{\partial t} = \frac{Q}{c\rho_o h_s} \qquad (9)$$

Hence changes in mixed layer temperature (and SST) are linearly related to the local net heat flux at the surface. When this type of model is used in a non-interactive context (ie. imposed fluxes with no feedback) the mixed layer temperature variation will not be cyclic over the annual cycle when the annual mean net surface heating is non-zero.

Figure 4 shows the differences between the seasonal range as simulated in the run and the climatological values shown in Figure 2. In the Northern hemisphere the simulated range is generally overestimated at low latitudes and underestimated at higher latitudes reflecting to some extent the heating/cooling trends due to the omission of any representation of lateral heat transport away from Equatorial regions. However in mid-latitudes the significant effects of advection would be expected to be limited to the boundary current regions (Gulf Stream and Kuroshio) and a more important factor in open ocean regions is the mis-representation of the shallow summer mixed layer. This is prevalent in the North Pacific where the simulated range is underestimated by more than 5°C extensively.

The Southern hemisphere characteristics are somewhat different and less extreme in magnitude. Lateral advective processes do not play such a significant role in local heat budget calculations since, unlike in the Northern hemisphere, there are no major meridional heat transporting systems. The range is underestimated generally in mid-latitudes but there are broad regions south of 45°S where the simulated range is in excess of 2°C over the climatological value. In these regions the latter is about 1°C although analysis of the fluxes for the period September to February shows that there is a large net heat gain. In the slab model this heat is distributed over 68m whereas observed mixed layer depths are typically much greater as will be seen later. Subsequent experiments to be described in this paper should confirm whether this could account for the overestimated seasonal ranges found in these regions.

B. Uniform depth ocean with a representation of advective effects

We now extend the slab model to include a representation of advective heat flux. However, in such a simple model we do not explicitly calculate these effects but instead make an attempt to prescribe them through some alternative method. Information regarding the magnitude of advective heat flux in the oceans is limited and estimates are usually made for latitude bands in meridional heat transport calculations (e.g. Oort and Vonder Haar, 1976). At this point in time no global datasets are available to enable us to prescribe directly the advective heat flux convergence at each grid point. An estimate of this quantity in the annual mean can be made, however, using the fluxes already at hand.

If we assume that there is no long term trend in the heat content of the upper ocean then from equation (6)

$$\frac{\bar{Q}}{c\rho_o} = \overline{h(\underline{U}_e.\underline{\nabla}T_m)} + \overline{\underline{U}_g.\underline{\nabla}\int_{-d}^{o} T dz} + \overline{W_{-h}(T_m - T_{-d})} \qquad (10)$$

This equation relates the annual mean net heat flux ($\bar{Q}$) at a point to the annual mean advective components. In mid-latitude open ocean regions we can ignore the geostrophic term and the upwelling term (Gill and Niiler, 1973, Barnett, 1981). If we also assume that seasonal Ekman affects are small [ie. $(h(\underline{U}_e.\underline{\nabla}T_m))' \approx 0$] then in this case, since the mixed layer depth is fixed at h_s we can specify an instantaneous value for the advective heat flux

$$\frac{\bar{Q}}{c\rho_o h_s} = \underline{U}_e.\underline{\nabla}T_m \qquad (11)$$

which can be incorporated into equation (3) such that

$$\frac{\partial T_m}{\partial t} + \frac{\bar{Q}}{c\rho_o h_s} = \frac{Q}{c\rho_o h_s} \qquad (12)$$

(if seasonal geostrophic effects are ignored).

$\bar{Q}$ is assumed to be positive downwards so equation (11) implies that an annual mean net heat loss to the atmosphere, for instance, will be compensated exactly by an annual mean net heat gain through advective heat flux convergence attributed in this case to horizontal Ekman advection, assumed constant over the annual cycle.

Figure 5 shows global values of $\bar{Q}$ from Esbensen and Kushnir (1981). The Gulf Stream and Kuroshio stand out as regions of implied annual mean warm advection with values in excess of 100 Wm^{-2} in the former case. In sub-tropical regions $\bar{Q}$ is positive generally as one would expect (ie. net heat gain by the ocean over the annual period). However the approximations used above cannot be applied to the mixed layer heat budget in the forementioned regions so any implications based on equation (12) will be invalid. Similar arguments apply to the boundary regions (although most of these are masked out in our experiments). In the Southern hemisphere, $\bar{Q}$ is generally small and negative apart from the South Atlantic Ocean where values are positive. The magnitude of $\bar{Q}$ in the Southern hemisphere reflects the absence of large scale meridional heat transport.

With this simple form of horizontal Ekman advection included the model was again run over the respective heating season of each hemisphere. The seasonal range difference for this experiment is shown in Figure 6. In mid-latitude regions in both hemispheres there has been a slight improvement but the differences are still large especially in the North Pacific. These results confirm that an important factor to consider, especially in the Northern hemisphere, is a representation of shallowing during the heating season.

In the Tropics the simulation has improved considerably although this is to be expected since the heating trend over the annual cycle has been removed.

C. Variable depth ocean with no advection

Having noted the results from the previous experiment we now ignore advective fluxes and introduce a seasonally varying mixed layer depth to replace the simple slab approach. Hence from equation (5)

$$\frac{\partial T_m}{\partial t} = \frac{Q}{c\rho_o h(t)} \qquad (13)$$

Changes in mixed layer temperature will therefore be no longer simply related to the net surface heat flux. An explicit determination of the mixed layer depth through a parametrization of mixing processes cannot be used here for reasons given in Section 4. Instead a diagnostic approach is sought using climatological temperature profiles primarily based on bathythermograph data.

The definition of the mixed layer depth is somewhat subjective but for the purposes of these general sensitivity tests we use a simple definition for h such that

$$T_{-h} = T_{surface} - 1°C \qquad (14)$$

We expect this criterion to provide reasonable estimates of mixed layer depth during the heating season at mid-latitudes when the mixed layer is usually well defined in terms of the vertical temperature profile (see Figure 2). Bathen (1972) used varying criteria and found reasonably good agreement between them under such conditions. During the winter months, however, there can be little variation of temperature with depth, especially at higher latitudes, although this does not necessarily imply that convective overturning occurs throughout the complete column because salinity gradients have increasing effect on the density structure at lower

temperatures. For instance, in the North Pacific there is a strong halocline below 150 metres which inhibits deep convection. Under these conditions a criterion based on temperature alone will overdeepen the mixed layer.

Seasonal means of mixed layer depth have been diagnosed from global ocean temperature analyses (Levitus and Oort, 1977) using the above definition. Figures 7,8,9,10 show the mixed layer depth distributions for each season. The evolution of the shallow mixed layer during the heating season can be clearly seen in the Northern hemisphere outside the Tropics. In the North Pacific the fields shown here can be compared with those obtained by Bathen (1972). In general there is good agreement when the mixed layer depths are shallow (consistent with Bathen's own observations mentioned above). Our values are also consistent with recent monthly mixed layer depth fields presented in Levitus (1982).

The seasonal evolution of the mixed layer depth field in the Southern hemisphere is not as pronounced. During the heating season mixed layer depths are greater than 25m in mid-latitudes apart from those regions which coincide with the locations of the sub-tropical high pressure cells (See Figure 11). It is noted that there are some spurious values in the Southern hemisphere which will affect the simulation at those points. These are at or near the ice edge and have been estimated using very limited data. For the purposes of this note they are best ignored.

To specify monthly mean mixed layer depth fields we have assumed that the seasonal values are representative for the middle of the three months in each case and have linearly interpolated to obtain values for each intermediate month. This is a rather crude approximation which will be expected to keep the mixed layer too deep in the early heating season at mid-latitudes (see Figure 12). The use of diagnostic mixed layer depth values in equation (13) is valid provided that the layer is shallowing. By specifying such values based on climatological ocean data a climatological estimate of the monthly mean turbulent mixing energy is loosely implied (see Gordon and Bottomley, 1984).

The results from this experiment are again shown as simulated - climatological range differences in Figure 13. In the Northern hemisphere, away from Equatorial regions and coasts, the differences are generally less extreme compared to those in experiments A and B although over much of the

North Pacific the range is still underestimated by more than 2°C. The spatial patterns, however, are somewhat different. The combination of a shallow mixed layer and large net downward heat flux in the central North Atlantic has led to higher SSTs than those observed. A more extreme example of this is seen in the central South Atlantic where the shallowest mixed layer depth given by our criterion is 12 metres for December. Combined with a downward heat flux of around 110 Wm^{-2}, this leads to a simulated SST rise of 4.5°C from December to January compared with a climatological rise of 1.6°C. Elsewhere in the Southern hemisphere the simulation has improved slightly although the introduction of observed mixed layer depths has not made a dramatic impact (e.g. the extensive area in the South Pacific where the range is underestimated by more than 2°C). The only exceptions are in the areas mentioned previously, south of 45°S, where the 68m slab model grossly overestimates the seasonal range.

In Equatorial and coastal regions there has been a marked deterioration in the simulation because of heating trends which have not been removed as in the previous experiment. As a consequence the excess heat is assumed to be distributed over the mixed layer which is generally shallow in such regions.

D. Variable depth ocean with advective flux convergence in the mixed layer

With a variable mixed layer depth the specification of an advective flux and its effect on changes in mixed layer temperature (and therefore SST) becomes more difficult. If we again use equation (10) and consider only horizontal Ekman effects then

$$\frac{\overline{Q}}{c\rho_o} = \overline{(h\underline{U}_e.\underline{\nabla}T_m)} \qquad (15)$$

The problem is now to specify an instantaneous advective heat flux. If we use equation (11) as in the slab model case then the assumption made implies that

$$(h\,\underline{U}_e.\underline{\nabla}T_m)' \approx 0 \qquad (16)$$

The validity of this assumption is open to question since h' is non-zero. However we shall incorporate advective effects in this way for this experiment and thus use equation (12) with h replacing h_s. (N.B. The advective heat flux convergence, assumed constant over the year, will be

concentrated within the variable mixed layer. As the layer shallows, the temperature change due to advection will increase hence enhancing the seasonal signal in mixed layer temperature).

Figure 14 shows the simulated-climatological seasonal range patterns from this experiment. Over most of the mid-latitude open ocean in the Northern hemisphere the results are encouraging and differences are within $\pm 2°C$. In regions where lateral advection is expected to be more important locally, the simulated range is overestimated and this is almost certainly due to the implied seasonal advective effects. The patterns in the Southern hemisphere have changed little from the previous experiment since $|\bar{Q}|$ is generally small away from Equatorial and coastal boundary regions. The large overestimations in the central South Atlantic still occur, therefore.

E. Variable depth ocean with constant heating in the mixed layer by advective fluxes

In this second experiment we specify the advective flux convergence in such a way that the heating rate due to advection over the mixed layer is constant. We assume that

$$\overline{h\underline{U}_e.\underline{\nabla}T_m} \approx \bar{h}\,\overline{\underline{U}_e.\underline{\nabla}T_m}$$

so that

$$\overline{\underline{U}_e.\underline{\nabla}T_m} \approx \frac{\bar{Q}}{c\rho_o\bar{h}} \qquad (17)$$

If seasonal variations in Ekman flux are small in mid-latitude open oceans (Gill and Niiler, 1973) then an instantaneous value can be specified and, from equation (3), over the heating season we obtain

$$\frac{\partial T_m}{\partial t} + \frac{\bar{Q}}{c\rho_o\bar{h}} = \frac{Q}{c\rho_o h} \qquad (18)$$

The seasonal range difference chart from this experiment is shown in Figure 15. It is interesting to note that the seasonal range has been underestimated in the North-west Atlantic and over a slightly more extensive area in the North Pacific (c.f. Experiment D). In these areas the simulation is sensitive to the advective flux specification and a model with explicit advective effects might perform better in such circumstances. Our method of relating $\bar{Q}$ to annual mean heat advection is probably a good

approximation for determining broad scale seasonal changes in the heat content of the upper ocean above the permanent thermocline (Gill and Niiler, 1973). However, to determine heat content changes in the mixed layer using a similar method requires an assumption to be made as to how the heat, attributed to advective flux convergence, is distributed within the upper ocean water column. (Similar arguments also apply in the Tropics if no inter-annual variability in heat content of the upper ocean is assumed).

Over much of the mid-latitude ocean, excluding the above areas, there is little difference between the broad scale patterns from experiments D and E which suggests that the precise form by which advective effects are included is not too important in these simple experiments.

6. Analysis of specific areas

In the modified slab model the approximations used in the specification of mixed layer depth and advective heat flux provide obvious sources of error although these are difficult to quantify. One of the purposes of this type of analysis is to ascertain to what extent the approximations have broken down. Another source of error, of course, is in the forcing fluxes themselves. Mitchell (1977b) has noted that large discrepancies often arise between estimates of the surface heat balance from various sources. Esbensen and Kushnir have discussed their methods of estimation and possible sources of error in the heat budget components. A major source of disagreement amongst authors involves the formulation of the cloudiness factor on which estimates of the radiative fluxes strongly depend. A criticism of Berliand's formula for incoming solar radiation at the surface, is its dependence on total cloud cover. Kasten and Czeplak (1979) concluded that, at any given location, the surface solar flux would largely depend on the frequency of occurrence of different cloud types rather than on total cloud cover alone. Errors in the turbulent fluxes using bulk formulae are believed to be between 10 and 20%. In view of these deficiencies, however, Esbensen and Kushnir state that the data are adequate for heat budget studies on a global scale although they point out that values south of 50°S should be treated with caution due to sparsity of data.

The results from experiments D and E show that a modified slab model can simulate the warming phase of the seasonal cycle to within 2°C over much of the global ocean. Differences of greater magnitude are mostly found in regions where one-dimensional processes would not be expected to dominate the local heat budget (e.g. boundary current regions). There are a few open mid-latitude ocean areas, however, where the model has not done as well as expected. In this section we look at two specific areas in greater detail.

(i) Central South Atlantic Ocean (specific point 28.75°S, 5.625°W)

In this region the range has been overestimated with the maximum deviation from climatology found at the above point (see Figure 13, for instance). The simulated range is given as 10.7°C at this point compared to an observed value of 5.4°C. The implied advective effects act as a weak heat sink in the South Atlantic but these are negligible when compared to the magnitude of the net downward heat flux across the surface during the heating season. Table 1 shows the monthly climatological and simulated SST changes from experiment E at 28.75°S, 5.625°W, together with the heat budget components and diagnosed mixed layer depths. During December and January there is a substantial net downward heat flux at this point which is distributed within a shallow mixed layer. In the simulation this leads to a SST rise of 8.2°C from November to January compared to a climatological rise of only 3.4°C. A study of the diagnosed mixed layer depth field shows that there is an elongated E-W band along 30°S where mixed layer depths are less than 20 metres during December. (To the north and south of this band values are more typically 30-40 metres). The larger overestimations of seasonal range, given by the simulation, do tend to coincide with the band suggesting, perhaps, that the diagnosed mixed layer depths are too shallow. Using equation (18) we can compute an approximate mean value for h which would correspond to a climatological SST rise from November to January, assuming that the fluxes are correct and advective effects are negligible. If this is done a value of around 40m is obtained. Alternatively, if the mixed layer depths are assumed to be representative, then the implied net downward heat flux would need to be around 40-50 Wm^{-2} to achieve climatological SST changes. This is 60-70 Wm^{-2} less than the climatological values from Esbensen and Kushnir (1981) shown in Table 1. It seems unlikely that the fluxes will exhibit errors of this magnitude.

In Section 4.1 we noted that the penetrative component of the incoming solar radiation is assumed to be completely absorbed within the mixed layer. This assumption begins to break down, however, as the layer shallows and a greater proportion of the solar beam can penetrate down through the mixed layer to heat the water beneath (see Woods, 1983). The absorption characteristics of sea water vary according to water type which typically for the South Atlantic is IA/IB. Using the absorption coefficients given in Paulson and Simpson (1977) it is estimated that about 16% of the incoming solar beam penetrates below a 15 metre mixed layer, for example. At the above location this could amount to ~40 Wm^{-2} during December and January using the solar radiative fluxes given in Table 1. If this is the case then it would partly account for the large overestimations which occur in mixed layer temperature. It will be of interest to see how well a Kraus-Turner type mixed layer model, which includes the effects of penetrative radiation, can perform in this region given the same fluxes and a representative dataset of wind-induced mixing.

(ii) North-eastern Pacific Ocean (specific point 51.25°N, 144.375°W)

This is an example of an area where the simulated range is less than climatology in each of the experiments described in the previous section. $\bar{Q}$ is generally negative in this area and large enough to affect monthly SST changes during the simulation. The simulated seasonal range obtained at this location therefore depends on the method by which the effects of advection are applied. However, even in the more extreme case, where the flux convergence is assumed to be in the mixed layer only (Experiment D) we find that the seasonal range is still underestimated by more than 2°C (see Figure 13). The point we have chosen for this study is at 51.25°N, 144.375°W, which is close to the old location of O.W.S.'P' where numerous studies of the local heat budget have been made. Table 2 gives the relevant data for this grid-point with the simulated monthly SSTs taken from experiment D. The predicted changes in SST are persistently lower than climatology suggests over the heating season with the largest underestimations occurring from April to June. It has already been noted that the mixed layer criterion used will cause overdeepening in the winter months and during the early part of the heating season (see Figure 12). By making a rough assumption that the error in SST is caused solely by the mixed layer depth criterion, we can again estimate the approximate mixed

layer depths which would be required to give climatological SST changes from April to June. This suggests depths of 20–30 metres throughout the period concerned. Climatological data from O.W.S. 'P' shows that the mixed layer does not become this shallow until later in the heating season. It seems appropriate to say that the mixed layer depth criterion accounts for part of the underestimation but errors in the fluxes and advective heat flux assumptions could be important. Once again it is difficult to quantify errors in the flux components but a simple error analysis on the fluxes, using the percentage errors quoted in Esbensen and Kushnir's atlas, shows that climatological SST changes could be achieved.

7. Discussion and conclusions

The primary aim of this study has been to provide some insight into the main factors which govern the climatological seasonal cycle of SST over the global ocean. This has, to some extent, been achieved by the series of sensitivity tests described here using observed forcing data. Our main interest has been in open mid-latitude ocean regions where local forcing is expected to dominate the heat budget of the upper ocean on the time and spatial scales relevant for climatological studies. Initial tests using a slab model failed to predict the seasonal range amplitude but subsequent modifications to include a seasonally varying mixed layer depth and a simple representation of advective flux convergence provided encouraging results. This is particularly true of mid-latitude oceans in the Northern hemisphere and leads to confidence, generally, in the quality of the forcing fluxes. In the Southern hemisphere the modifications to the slab model have a less dramatic impact and differences between the simulated and climatological seasonal range values are somewhat larger than originally expected. This might reflect poor quality in the flux estimates in some regions due to sparsity of data.

In Equatorial regions generally the approximations used in the experiments do not apply and the simulations obtained in such regions do not provide an understanding of the processes which may be important in determining mixed layer temperature changes. Similarly this is the case in boundary current regions. For these reasons a simple mixed layer model would not be considered suitable for coupled global ocean-atmosphere

experiments. It can, however, be of use in providing a diagnostic tool with which the quality of AGCM fluxes can be assessed in terms of model sensitivity.

In the near future it is planned to run similar experiments to those reported here using a Kraus-Turner type mixed layer model driven by climatological heat fluxes and a climatological estimate of wind-forcing derived from statistical parameters relating to monthly windspeed distributions (Grahame, 1984). The results from these experiments will be reported later.

Acknowledgements

I would like to thank Drs. Cattle and Gordon for their help and comments.

References

Ballis, D.J., 1975: Monthly mean bathythermograph data from O.W.S. "PAPA", S.I.O. Reference Series, University of California.

Barnett, T.P., 1981: On the nature and causes of large-scale thermal variability in the central North Pacific Ocean. J. Phys. Oceanogr. 11, 887-904.

Bathen, K.H., 1972: On the seasonal changes in the depth of the mixed layer in the North Pacific Ocean. J. Geophys. Res., 77, 7138-7150.

Budyko, M.I., 1974: Climate and life. Academic Press, 508 pp.

DeSzoeke, R.A., and P. B. Rhines, 1976: Asymptotic regimes in mixed-layer deepening. Journal of Marine Research, 34, 111-116.

Esbensen, S.K., and Y. Kushnir, 1981: The heat budget of the global ocean: An atlas based on estimates from surface marine observations. Report No. 29, Climatic Research Institute, Oregon State University, Corvallis.

Gill, A.E., and P.P. Niiler, 1973: The theory of the seasonal variability in the ocean. Deep Sea Research, 20, 141-177.

Gordon, C., 1984: Sensitivity tests with a simple mixed layer model. Dynamical Climatology Technical Note. (In preparation).

Gordon, C., and M. Bottomley, 1984: The parametrization of the upper ocean mixed layer in coupled ocean/atmosphere models. Dynamical Climatology Technical Note No. 2.

Grahame, N.S., 1984: A technique for representing synoptic-scale variability for calculations of monthly mean wind-forcing for mixed layer experiments. Met O 20 Tech. Note II/221.

Hellerman, S., 1967: An updated estimate of the wind stress on the world ocean. Monthly Weather Review, 95, 607-626.

Kasten, F., and G. Czeplak, 1980: Solar and terrestrial radiation dependent on the amount and type of cloud. Solar Energy, 24, 177-189.

Kim, J.-W., and W.L. Gates, 1980: Simulation of the seasonal fluctuation of the upper ocean by a global circulation model with an imbedded mixed layer. Report No. 11, Climatic Research Institute, Oregon State University, Corvallis.

Kraus, E.B., and J. S. Turner, 1967: A one-dimensional model of the seasonal thermocline. II. The general theory and its consequences. Tellus, 19, 98-106.

Levitus, S., 1982: Climatological atlas of the world ocean. NOAA Professional Paper 13. Geophysical Fluid Dynamics Laboratory, Princeton.

Levitus, S., and A. Oort, 1977: Global analysis of oceanographic data. Bull. Amer. Meteor. Soc., 58, 1270-1284.

Manabe, S., and R.J. Stouffer, 1980: Sensitivity of a Global Climate Model to an increase of CO_2 concentration in the atmosphere. J. Geophys. Res., 85, 5529-5554.

Mitchell, J.F.B., 1977a: An oceanic mixed layer model for use in General Circulation Models. Met O 20 Tech. Note II/85.

Mitchell, J.F.B., 1977b: Some experiments using a simple oceanic mixed layer model. Met O 20 Tech. Note II/86.

Oort, A.H., and T.H. Vonder Haar, 1976: On the observed annual cycle in the ocean-atmosphere heat balance over the Northern hemisphere. J. Phys. Oceanogr., 6, 781-800.

Paulson, C.A., and J.J. Simpson, 1977: Irradiance measurement in the upper ocean. J. Phys. Oceanogr. 7, 952-956.

Schutz, C., and W.L.Gates, 1971: Global climatic data for surface, 800 mb, 400 mb: January. R-915-ARPA, The Rand Corporation, Santa Monica, CA.

Schutz, C., and W.L. Gates, 1972: Global climatic data for surface, 800 mb, 400 mb: July. R-1029-ARPA, The Rand Corporation, Santa Monica, CA.

Schutz, C., and W.L. Gates, 1973: Global climatic data for surface, 800 mb, 400 mb: April. R-1317-ARPA, The Rand Corporation, Santa Monica, CA.

Schutz, C., and W.L. Gates, 1974: Global climatic data for surface, 800 mb, 400 mb: October. R-1425-ARPA, The Rand Corporation, Santa Monica, CA.

Wells, N.C., 1979: A coupled ocean-atmosphere experiment. The ocean response. Q.J. Royal Meteor. Soc., 105, 335-370.

Woods, J.D., 1983: Climatology of the upper boundary of the ocean. In: Large-scale oceanographic experiments in the WCRP. Vol II. pp 147-179.

Table 1. Climatological data and predicted sea surface temperatures (Experiment E) at 28.75°S, 5.625°W.

		OCT	NOV	DEC	JAN	FEB	MAR
Climatological SST	(°C)	17.4	18.6	20.4	22.0	22.5	22.4
Simulated SST	(°C)	17.1	17.7	21.3	25.9	27.8	28.3
Available solar, F_S	(Wm^{-2})	170.5	209.0	245.1	261.6	219.1	188.7
Net I.R., F_I	(Wm^{-2})	-54.7	-54.6	-56.9	-59.0	-55.9	-57.7
Sensible heat, F_{SH}	(Wm^{-2})	-2.3	0.4	0.9	0.7	-1.7	-3.0
Latent heat, F_{LH}	(Wm^{-2})	-82.6	-71.6	-76.6	-92.1	-105.9	-108.3
Net downward heat flux, Q	(Wm^{-2})	30.9	83.2	112.5	111.2	55.6	19.7
$\bar{Q}$	(Wm^{-2})	2.8	2.8	2.8	2.8	2.8	2.8
Computed m.l.d., h	(m)	87.1	49.5	11.9	25.2	38.4	51.7

Table 2. Climatological data and predicted sea surface temperatures (Experiment D) at 51.25°N, 144.375°W.

		APR	MAY	JUN	JUL	AUG	SEP
Climatological SST	(°C)	5.7	6.8	9.0	11.3	13.2	10.8
Simulated SST	(°C)	5.5	5.7	6.9	8.8	10.4	11.3
Available solar, F_S	(Wm^{-2})	116.0	127.6	123.3	113.2	99.3	91.3
Net I.R., F_I	(Wm^{-2})	-45.2	-37.3	-31.0	-29.1	-31.5	-41.7
Sensible heat, F_{SH}	(Wm^{-2})	-2.8	4.9	6.4	5.2	2.9	0.0
Latent heat, F_{LH}	(Wm^{-2})	-39.3	-23.9	-18.1	-17.2	-28.9	-45.7
Net downward heat flux, Q	(Wm^{-2})	28.7	71.3	80.6	72.1	41.8	3.9
$\bar{Q}$	(Wm^{-2})	-14.6	-14.6	-14.6	-14.6	-14.6	-14.6
Computed m.l.d., h	(m)	223.4	127.8	32.1	30.0	27.9	25.8

In the above tables the surface flux components are from Esbensen and Kushnir (1981) with downwards taken as positive.

Figure Captions

Figure 1. Climatological seasonal range of sea surface temperature defined as:
August - March SST in the Northern hemisphere
February - September SST in the Southern hemisphere.
N.B. Using this definition there are some areas where the seasonal range is negative, notably between 0° and 5°N in the Eastern Equatorial Atlantic, Eastern Equatorial Pacific and Indian Ocean.

Figure 2. Upper ocean vertical temperature profile at O.W.S. "PAPA" (50°N, 145°W) for August 1966 (taken from Ballis, 1975).

Figure 3. Schematic temperature and velocity profile used in the derivation of equations in Section 4.1.

Figure 4. Seasonal range differences (simulated - climatological) for Experiment A - basic slab model with a 68m mixed layer depth.

Figure 5. Annual net downward heat flux, $\bar{Q}$ (taken from Esbensen and Kushnir, 1981).

Figure 6. Seasonal range differences for Experiment B - basic slab model with a representation of advective heat flux convergence incorporated.

Figure 7. Computed seasonal mean of mixed layer depth over the global ocean for February, March, April.

Figure 8. As Figure 7 but for May, June, July.

Figure 9. As Figure 7 but for August, September, October.

Figure 10. As Figure 7 but for November, December, January.

Figure 11. Mean sea level pressure for December (taken from Esbensen and Kushnir, 1981).

Figure 12. Monthly mean mixed layer depths over the annual cycle from Levitus (1982) and as calculated in the text. The latter clearly overestimates the mixed layer depth during the early heating season (i.e. April and May).

Figure 13. Seasonal range differences for Experiment C - variable depth mixed layer model. Mixed layer depths have been specified as monthly mean values.

Figure 14. Seasonal range differences for Experiment D - variable depth mixed layer model and a representation of advective heat flux convergence over the instantaneous mixed layer depth.

Figure 15. Seasonal range differences for Experiment E - variable depth mixed layer model and a representation of advective heat flux convergence over the annual mean mixed layer depth.

CLIMATOLOGICAL SST
SEASONAL RANGE

> 5°C

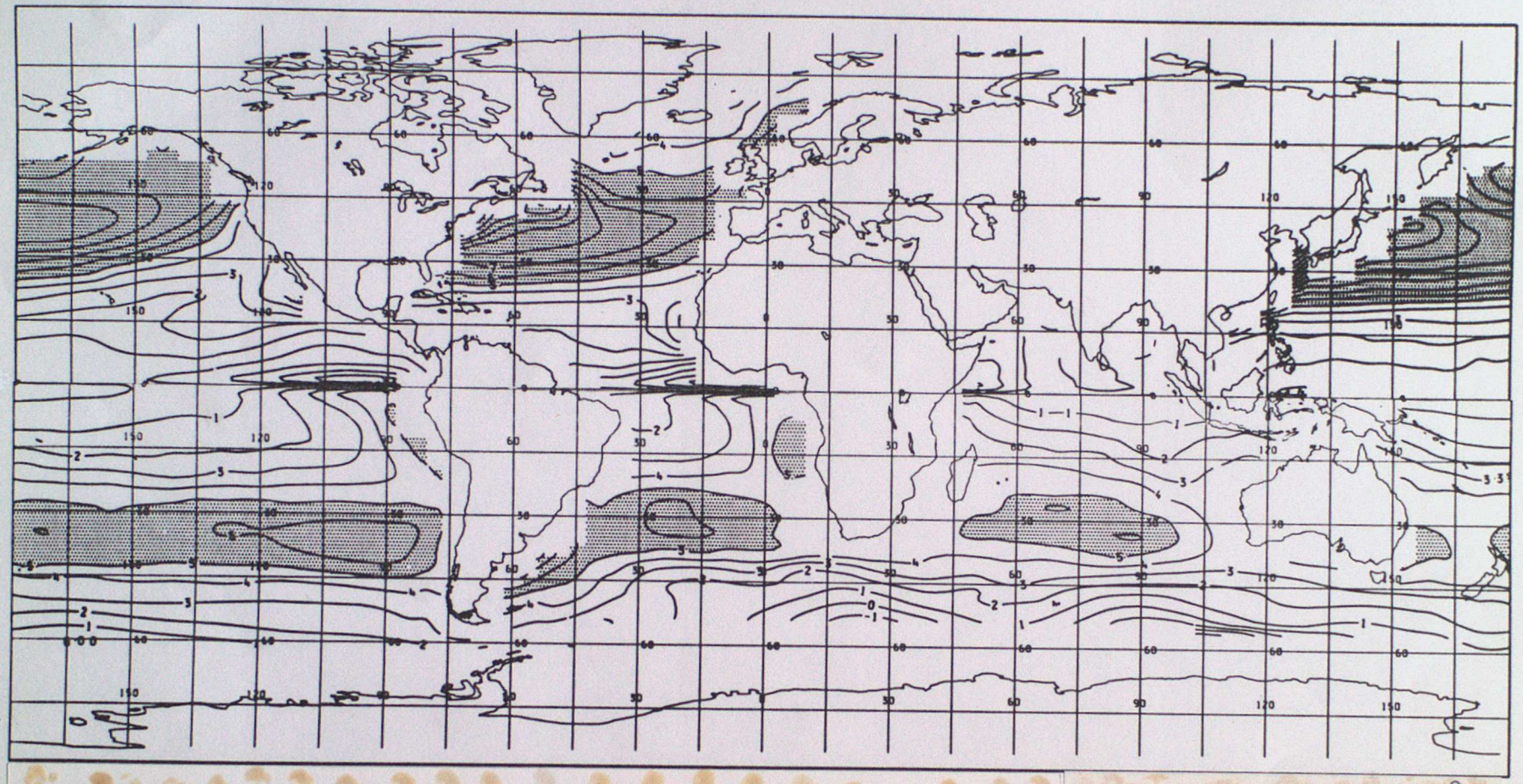

Contour interval=1°C

Figure 1: Climatological seasonal range of sea surface temperature defined as:
August - March SST in the Northern hemisphere
February - September SST in the Southern hemisphere.

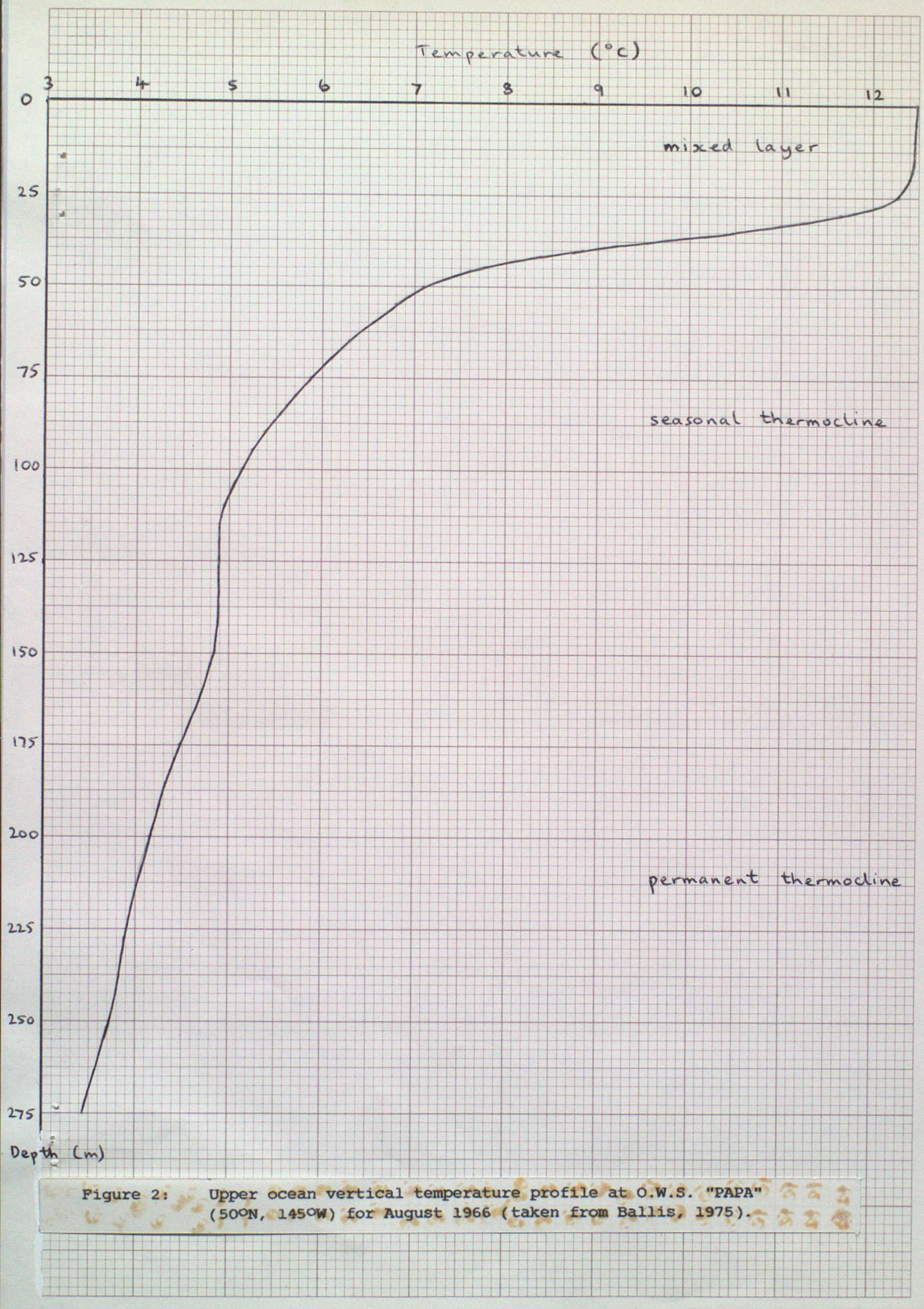

Figure 2: Upper ocean vertical temperature profile at O.W.S. "PAPA" (50°N, 145°W) for August 1966 (taken from Ballis, 1975).

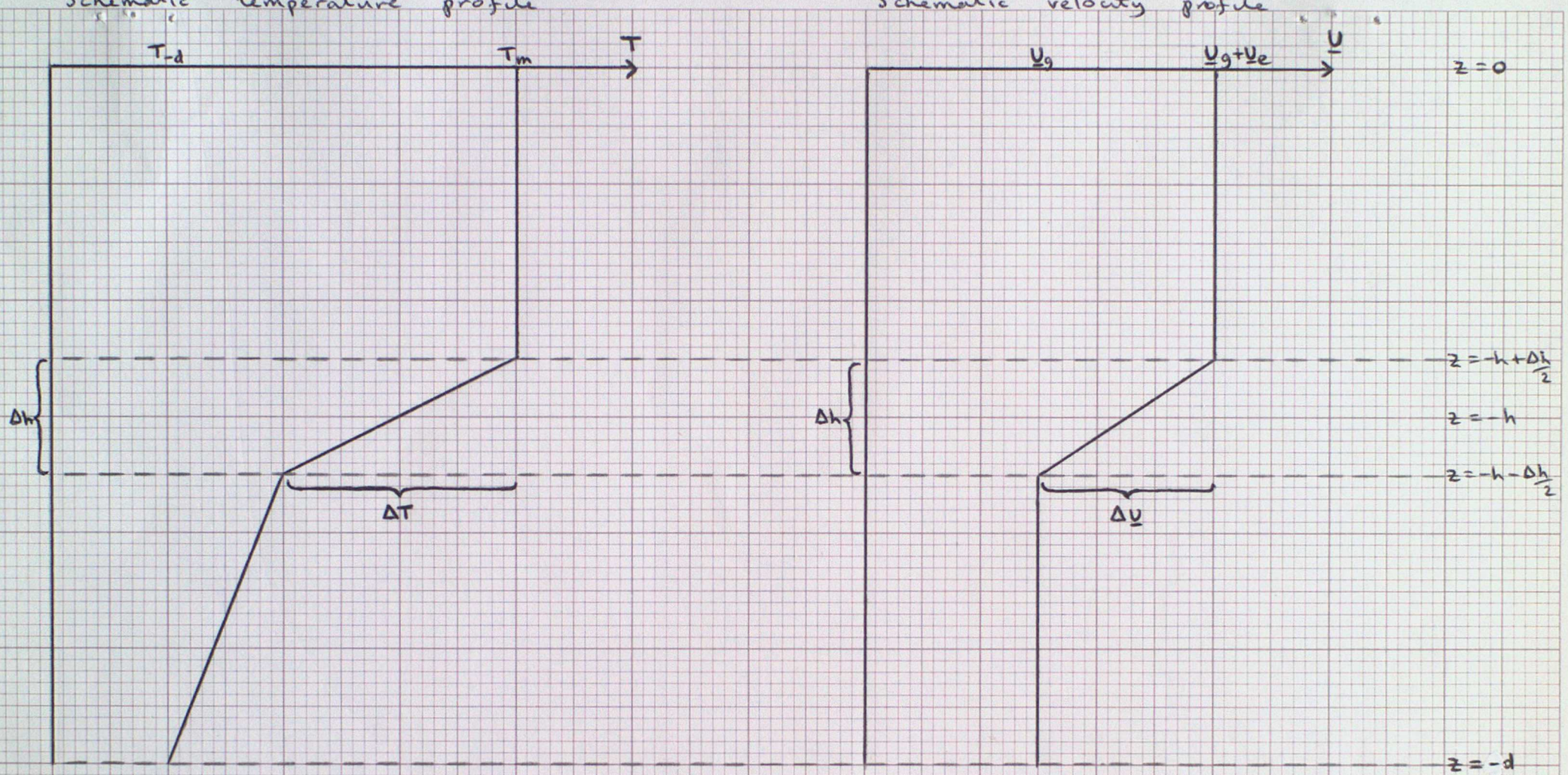

T_m is the temperature of the mixed layer

$\Delta T = T_{-h+\frac{\Delta h}{2}} - T_{-h-\frac{\Delta h}{2}}$

Depth, $-d$, is considered to be at the bottom of the seasonal thermocline

$\underline{U}_g$ is the geostrophic current (assumed constant with depth)

$\underline{U}_e$ is the Ekman current (assumed constant in the mixed layer)

$\Delta \underline{U} = \underline{U}_e$

Figure 3: Schematic temperature and velocity profile used in the derivation of equations in Section 4.1.

SEASONAL RANGE DIFFERENCE
SIMULATED-CLIMATOLOGICAL

EXP A

> 2°C

< -2°C

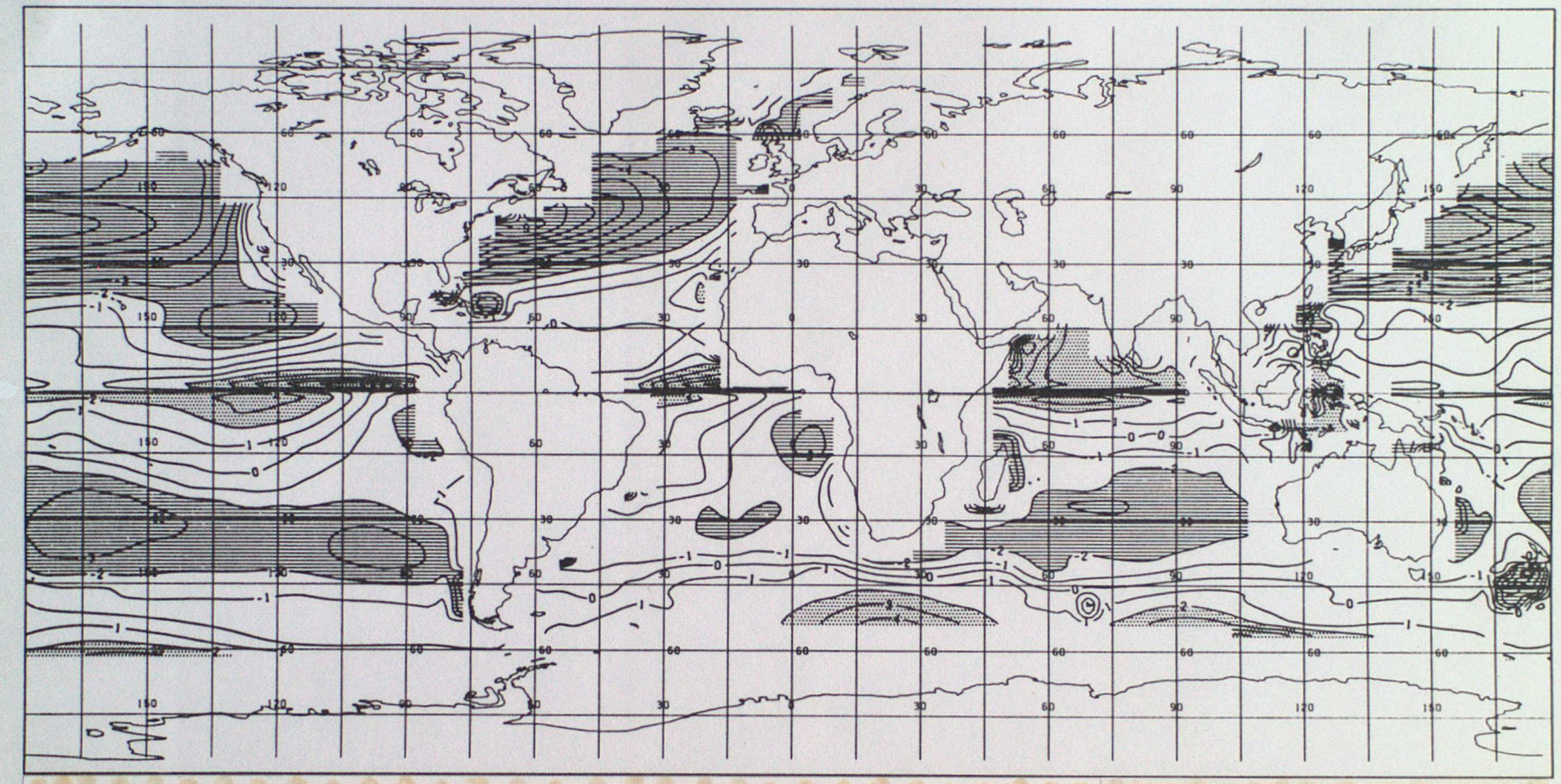

Figure 4: Seasonal range differences for Experiment A.

Contour interval=1°C

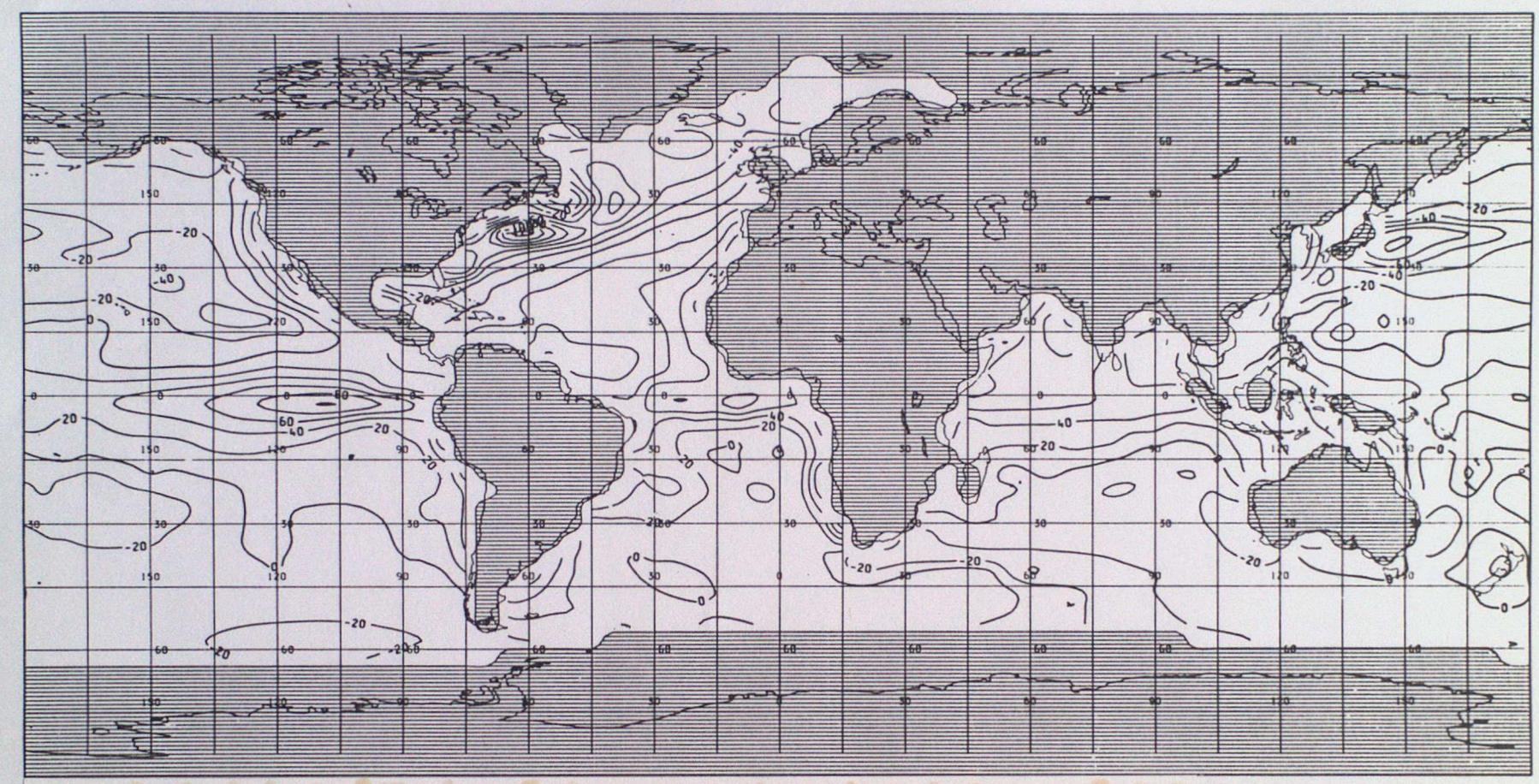

Figure 5: Annual net downward heat flux, $\overline{Q}$ (taken from Esbensen and Kushnir, 1981).

SEASONAL RANGE DIFFERENCE
SIMULATED-CLIMATOLOGICAL

EXP B

> 2°C

< -2°C

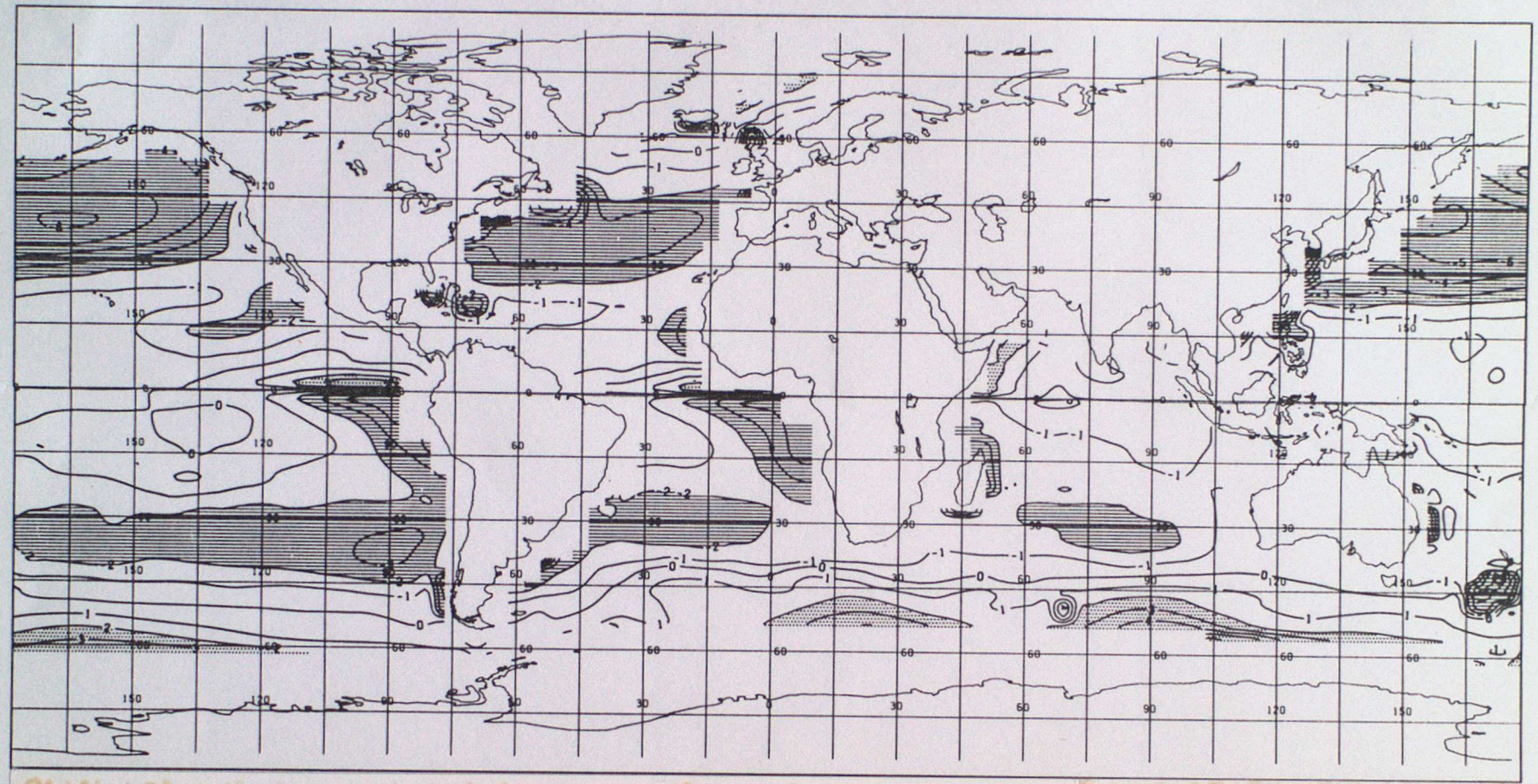

Figure 6: Seasonal range differences for Experiment B.

Contour interval=1°C

SEASONAL MEAN MIXED LAYER DEPTHS
UNITS:METRES

FEB.MAR.APR

< 25m.

> 100m.

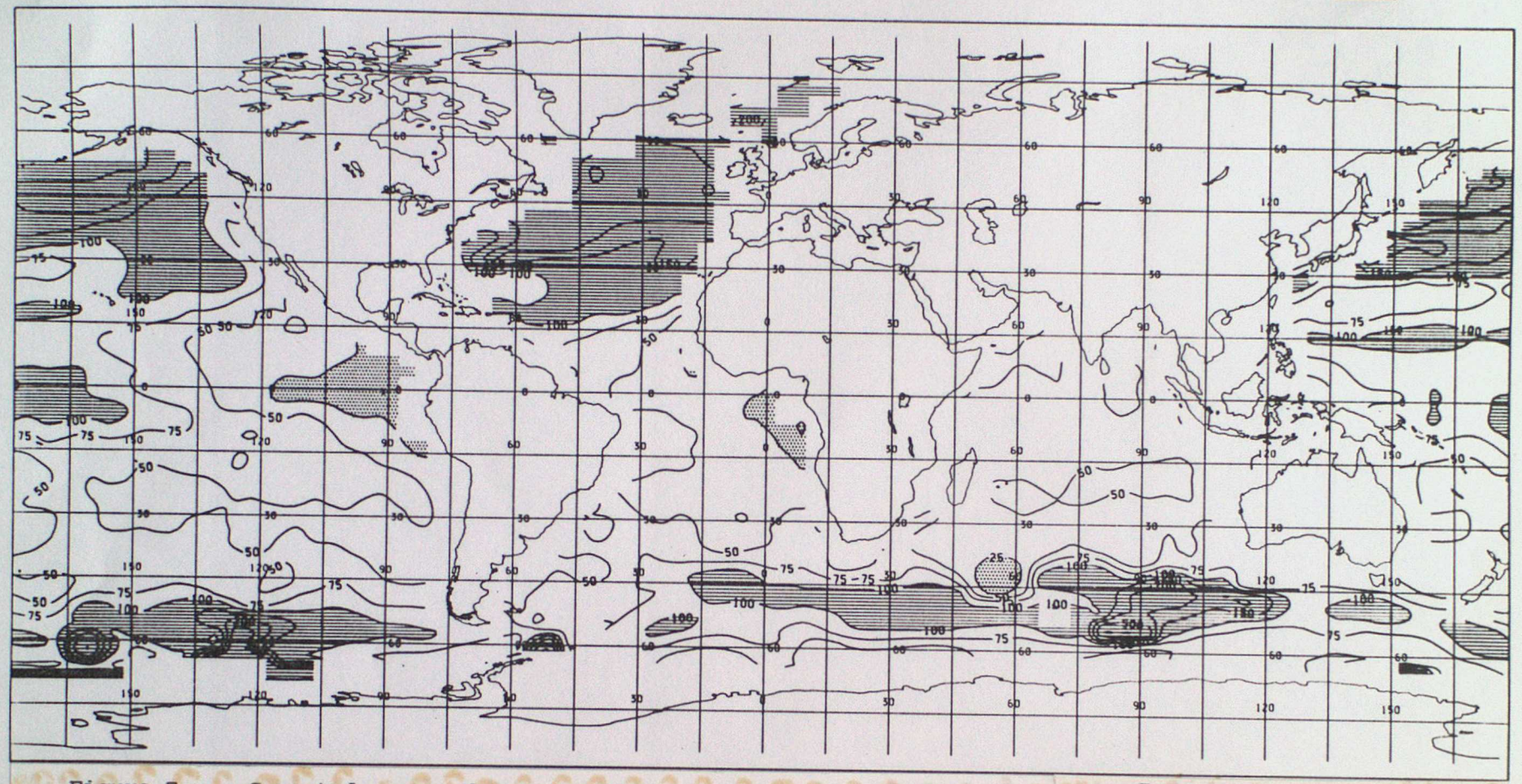

Figure 7: Computed seasonal mean of mixed layer depth for February, March, April.

Irregular contour interval

SEASONAL MEAN MIXED LAYER DEPTHS
UNITS:METRES

MAY.JUN.JUL

< 25 m.

> 100 m.

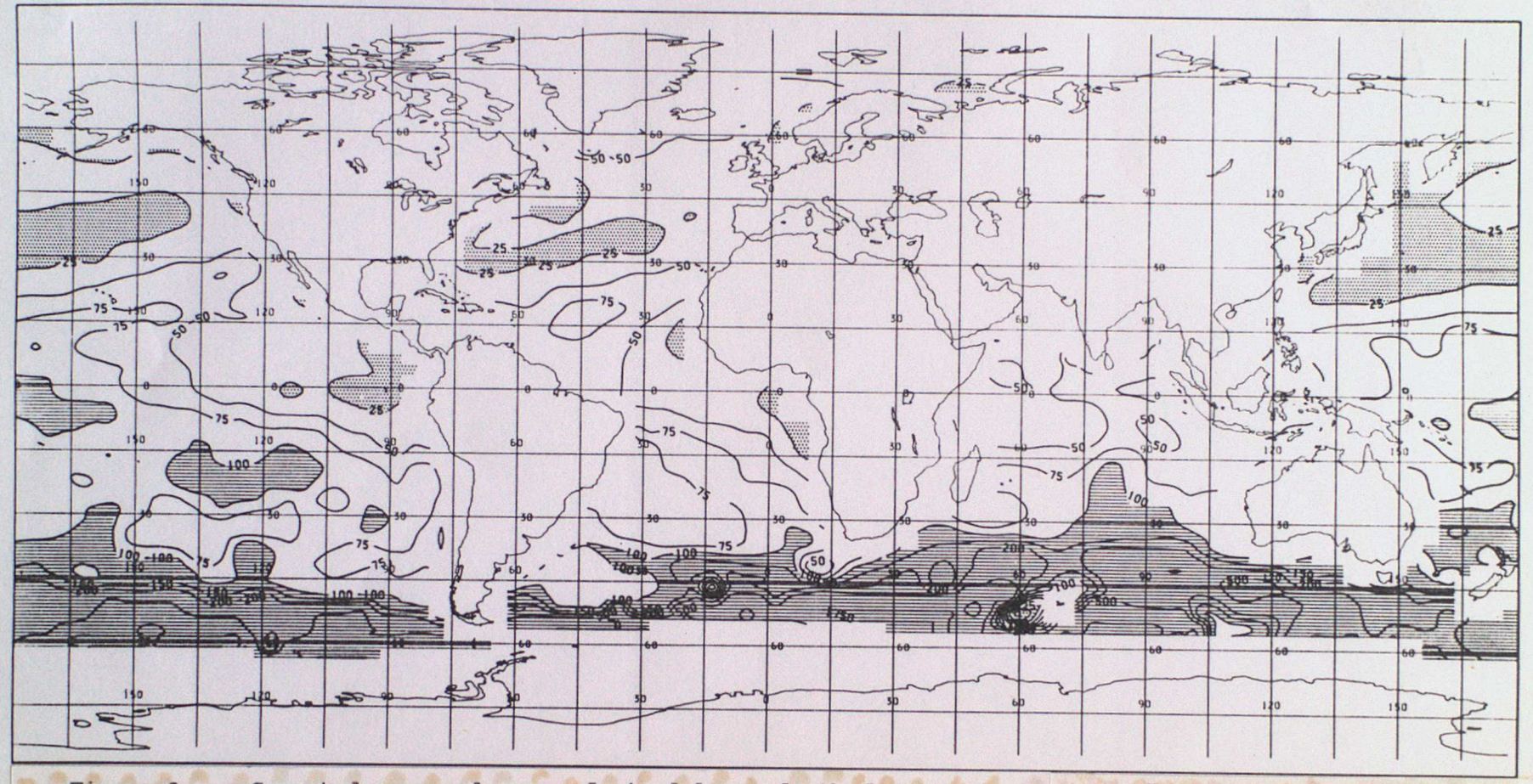

Figure 8: Computed seasonal mean of mixed layer depth for May, June, July. Irregular contour interval

SEASONAL MEAN MIXED LAYER DEPTHS
UNITS:METRES

AUG.SEP.OCT

< 25 m.

> 100 m.

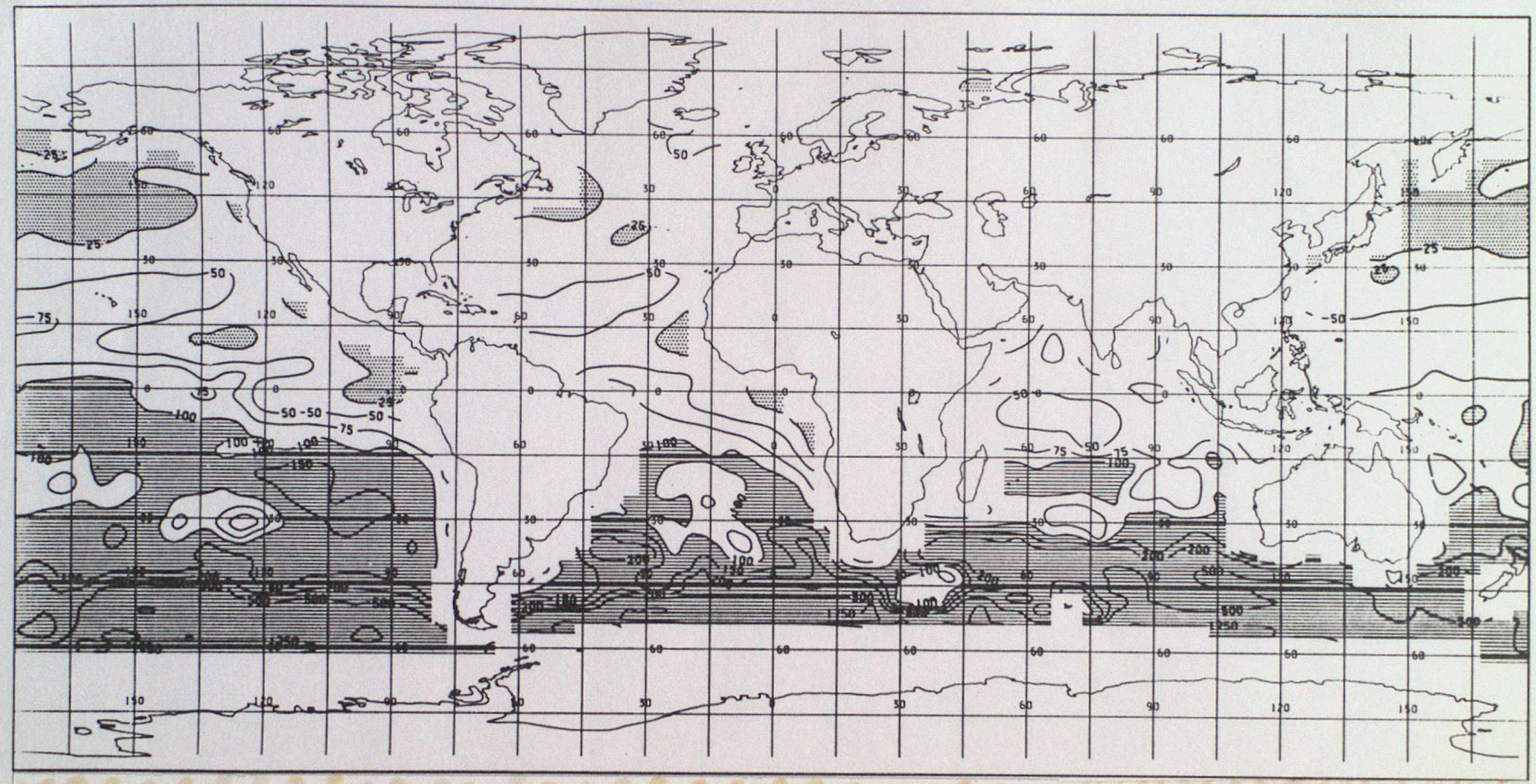

Figure 9: Computed seasonal mean of mixed layer depth for August, September, October.

Irregular contour interval

SEASONAL MEAN MIXED LAYER DEPTHS
UNITS:METRES

NOV.DEC.JAN

< 25 m.

> 100 m.

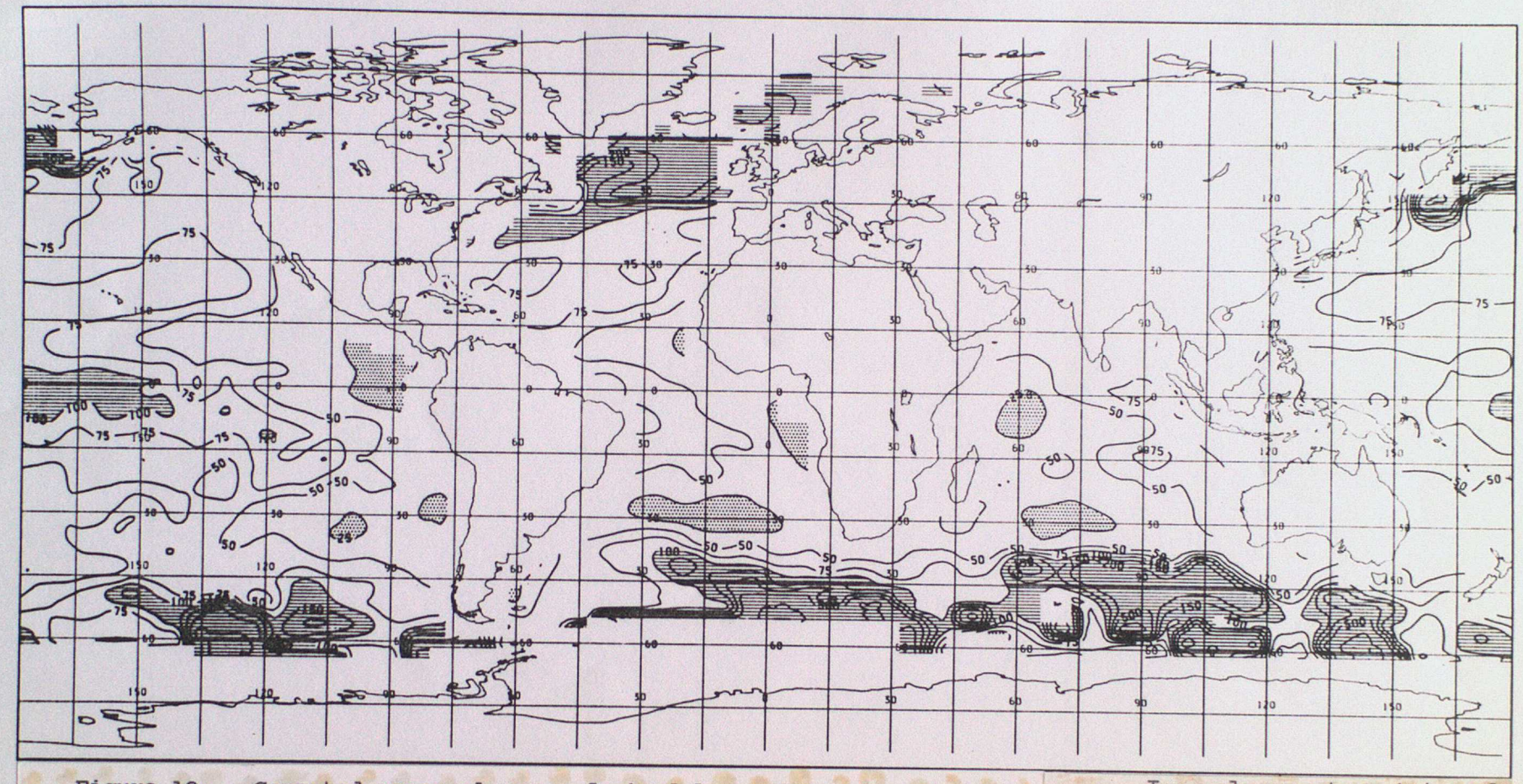

Figure 10: Computed seasonal mean of mixed layer depth for November, December, January.

Irregular contour interval

DECEMBER MSL PRESSURE (MB)

ESBENSEN + KUSHNIR
CONTOUR INTERVAL IS 4MB

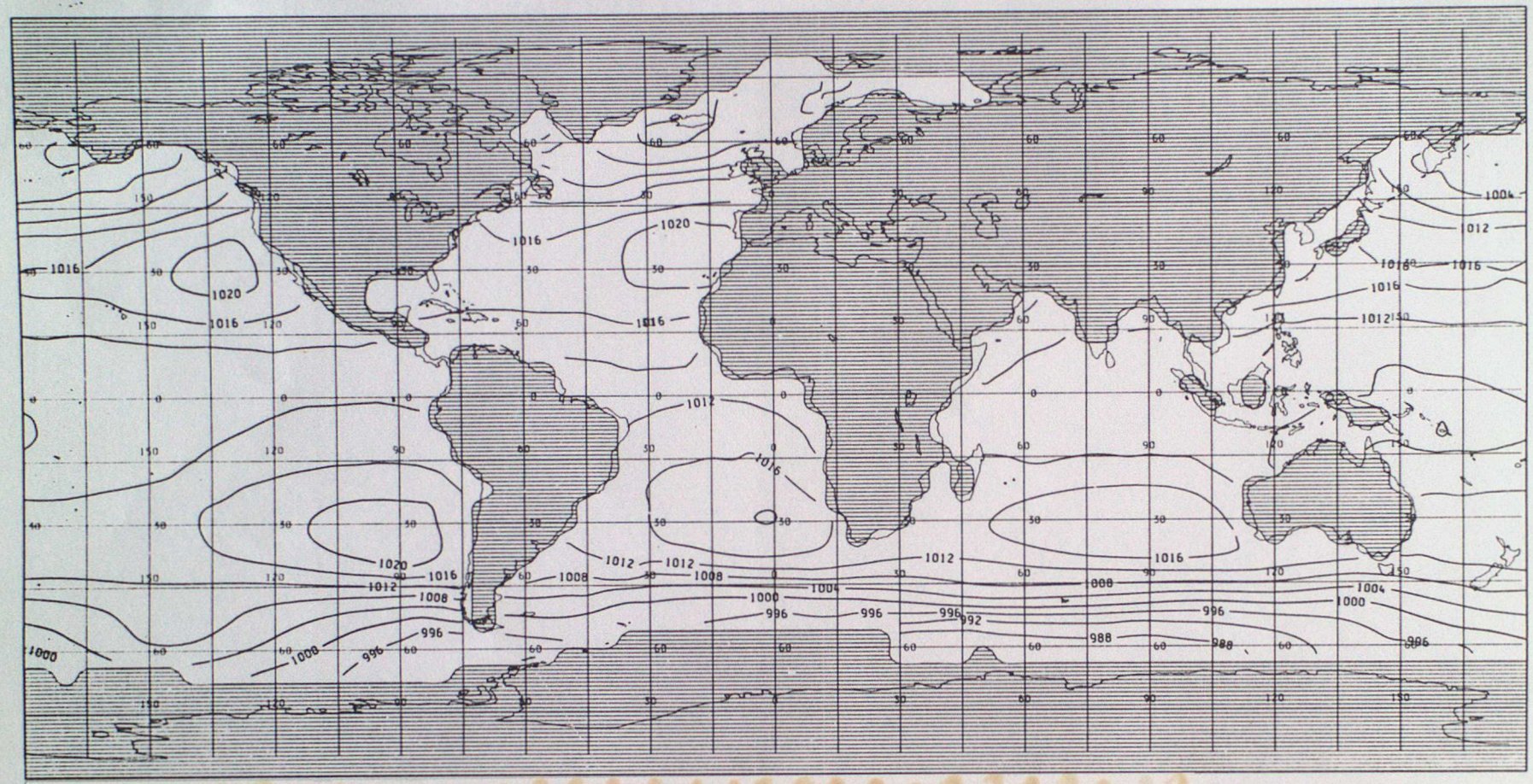

Figure 11: Mean sea level pressure for December (taken from Esbensen and Kushnir, 1981).

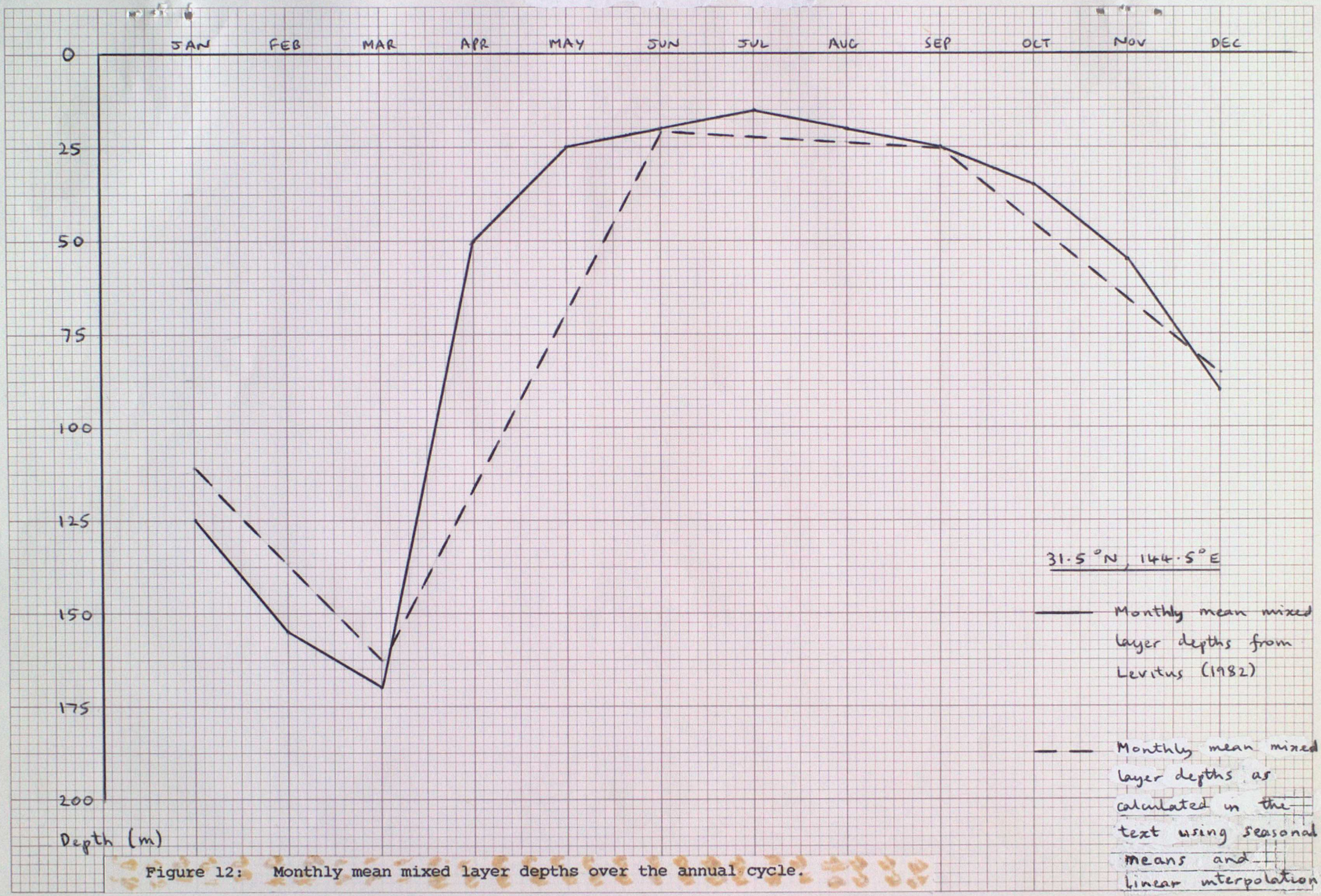

Figure 12: Monthly mean mixed layer depths over the annual cycle.

SEASONAL RANGE DIFFERENCE
SIMULATED-CLIMATOLOGICAL

EXP C

> 2°C

< -2°C

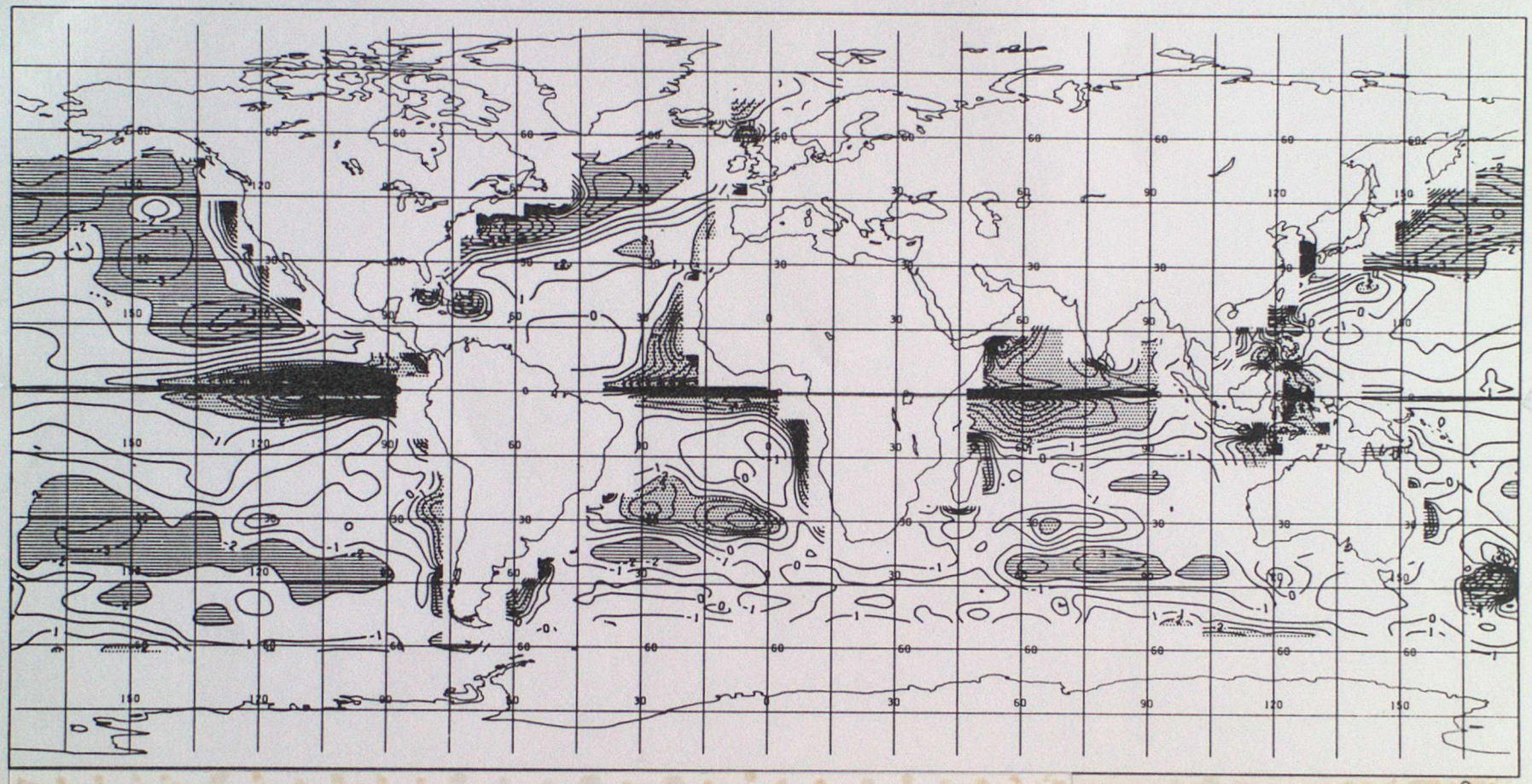

Figure 13: Seasonal range differences for Experiment C.

Contour interval=1°C

SEASONAL RANGE DIFFERENCE
SIMULATED-CLIMATOLOGICAL

EXP D

> 2°C

< -2°C

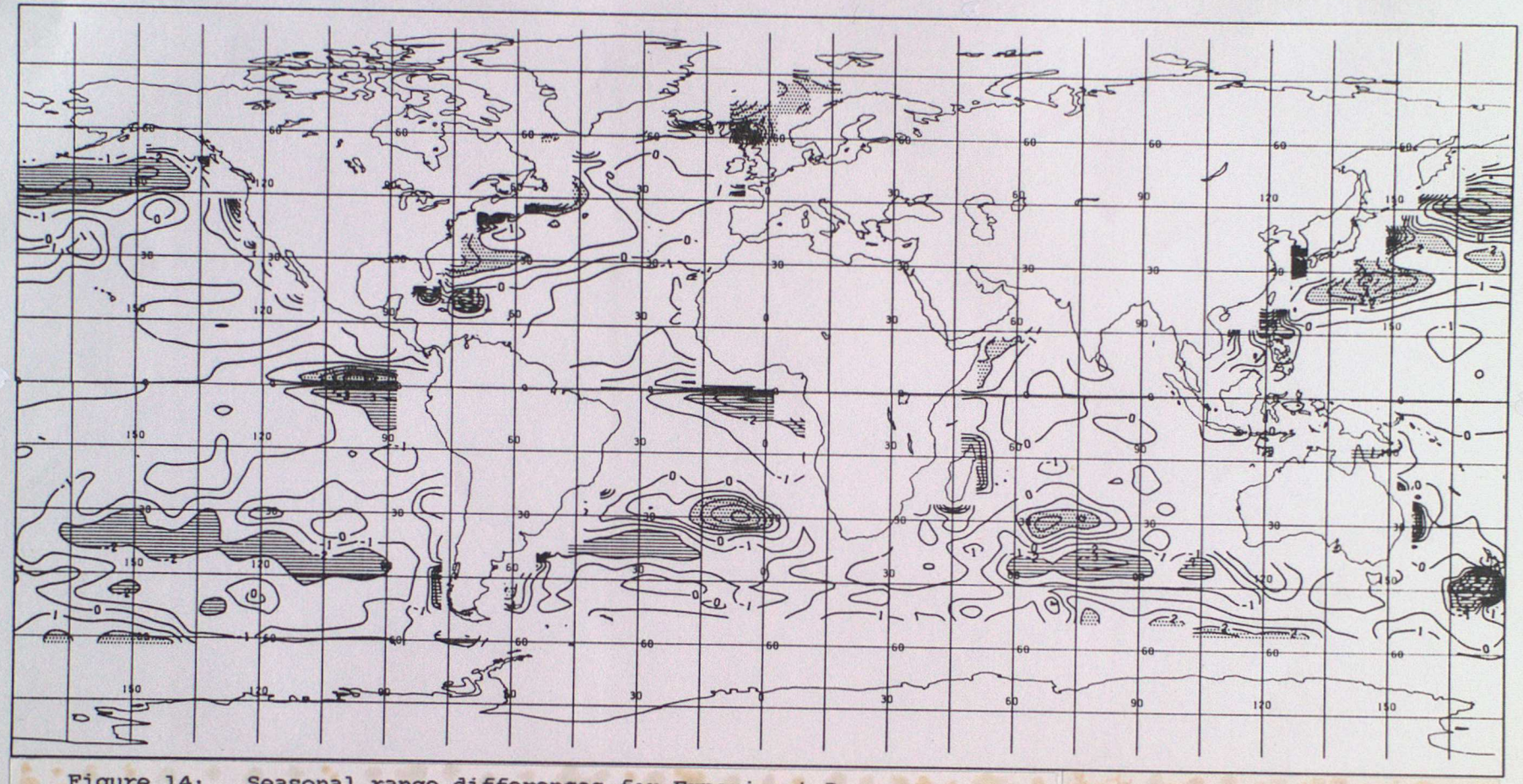

Figure 14: Seasonal range differences for Experiment D.

Contour interval=1°C

SEASONAL RANGE DIFFERENCE
SIMULATED-CLIMATOLOGICAL

EXP E

> 2°C

< -2°C

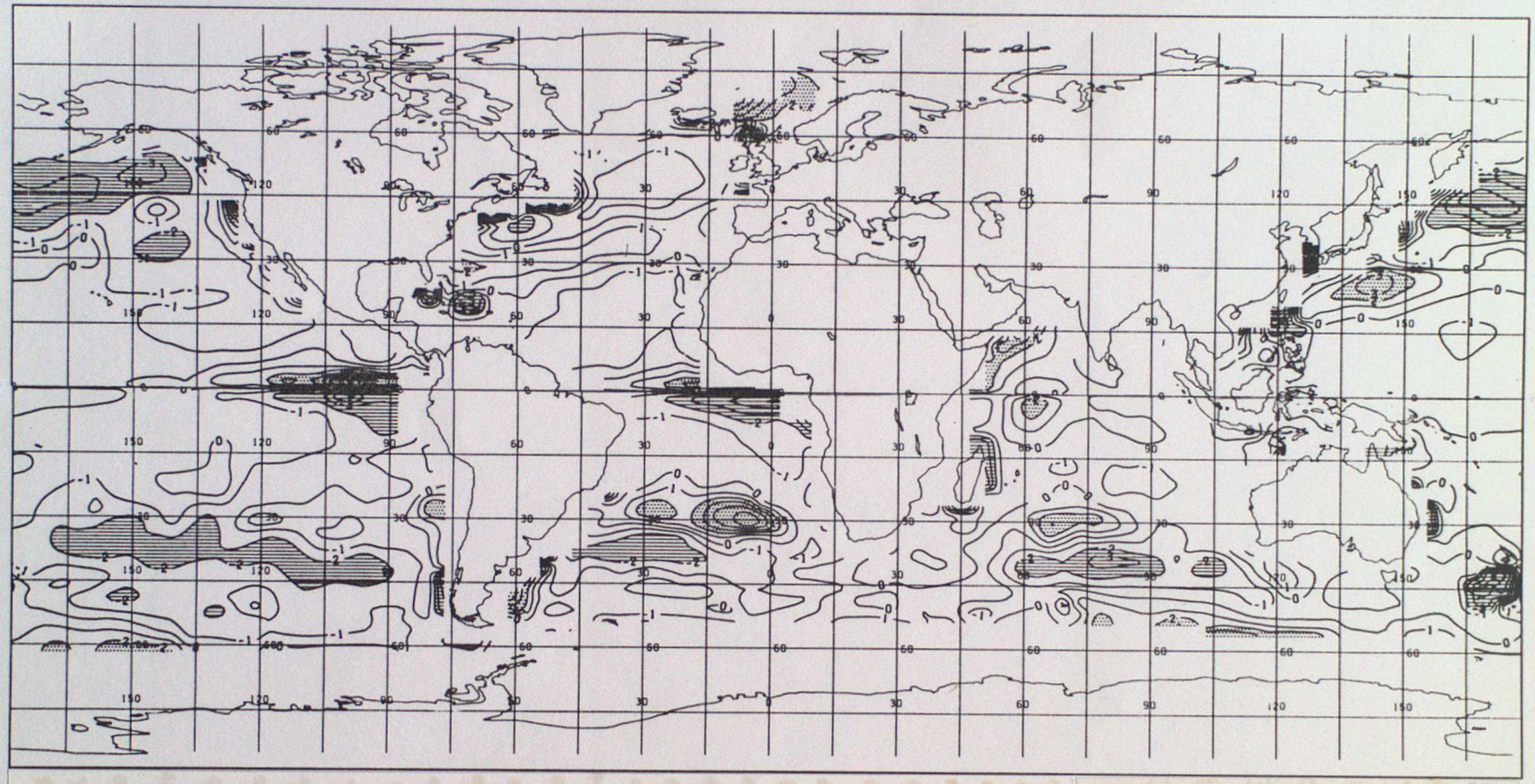

Figure 15: Seasonal range differences for Experiment E.

Contour interval=1°C